SolarPACES 2024, 30th International Conference on Concentrating Solar Power, Thermal, and Chemical Energy Systems

Solar Fuels and Chemical Commodities

https://doi.org/10.52825/solarpaces.v3i.2405

Published: 12 Dec. 2025

Continuous Solar Hydrogen and Syngas Production in Membrane Reactors

Nicole Carina Neumann[1,*], Juan Pablo Rincon Duarte[1], and Martin Roeb[1]

[1]German Aerospace Center (DLR), Germany

*Correspondence: Nicole Carina Neumann, Nicole.Neumann@dlr.de

Abstract. Satisfying the industry's growing demand for sustainable hydrogen requires the rapid development of a diverse mix of hydrogen production technologies. The membrane technology is capable of shifting the thermodynamic limits of water splitting to lower temperatures and thus into a technically feasible range. This thermodynamic limit was determined with respect to possible molar flow parameters and temperature, where biomethane is considered as reducing agent on the permeate side of the membrane or a purge gas dilutes the permeated oxygen concentration. In the second part of this study, a developed thermal model is used to analyse the integration of real solar flux distribution into a membrane stack reactor. To avoid failure of the joined membrane modules, a homogeneous temperature distribution (< 50 K) along the reactor body is required. However, the solar flux distribution from a solar system is characterised by a Gaussian-shape with a peak in its centre, which results in the generation of hot spots. Our model consists of a cavity, the reactor and a set of plates, which are used to enhance the temperature distribution in the reactor. It was found that parameters such as the aperture diameter of the cavity, the distance of the cavity to the focal point and the material of the irradiated plates influence the temperature distribution on the reactor stack. An aperture diameter of 55 mm and a distance of 135 mm to the focal point met the temperature requirements of the membrane stack reactor.

Keywords: Solar Hydrogen, Membrane Reactor, Thermal Simulation, Ray-Tracing.

1. Introduction

The world-wide demand of the industry for hydrogen and also syngas, as a precursor for many chemicals such as methanol or dimethyl ether, is expected to rise in future to i.e. 140 Mt/a hydrogen [1]. One promising sustainable solution for hydrogen or syngas production are solar-powered catalytic membrane reactors, which can split H_2O using oxygen transport membranes (see Figure). This oxygen transport membrane is a dense ceramic membrane with a mixed ionic-electronic conductivity where oxygen ions diffuse through the crystal lattice. One promising membrane material candidate is Fe-doped strontium-titanate, which provides a good compromise of mechanical stability an ambipolar conductivity for the respective temperature and oxygen partial pressure range.

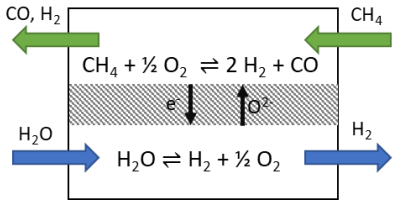

Figure 1. *Concept of a countercurrent membrane reactor for water splitting.*

In contrast to electrochemical approaches, this membrane-based process only requires heat and no electricity. Consequently, more cost-effective thermal energy storage systems can be used instead of electrical energy storage systems to ensure 24-7 operation [2]. The coupling of membrane technology with concentrating solar systems combined with thermal energy storages thus ensures a perspective of continuous operation based on renewable energies. The driving force of the water splitting reaction in the membrane reactor is the difference of oxygen partial pressure across the membrane. When (bio)methane is used as reducing agent on the permeate side, the temperature demand drops to around 850 °C. Even though the overall reaction equation is the same as for steam reforming, membrane technology enables a more flexible response to the requirements of downstream processes. The syngas ratio can be adjusted by mixing the two product gases, or pure H_2 and syngas (with a relevant 2:1 ratio) can be produced separately without WGS or separation processes. Alternatively, one can omit carbon and use a sweep gas to dilute the oxygen concentration on the permeate side. In this case, the membrane technology allows for a continuous isothermal production compared to the typical temperature swing of the two-step thermochemical cycle and thus it avoids potential energy loss due to the required heat recuperation step.

In this work, we firstly identify the thermodynamic limit of such a reactor depending on the operation conditions and secondly design the solar heat integration for a biomethane-supported operation of a membrane-stack reactor. Thermal simulations are carried out with different solar flux distributions as input to identify a suitable reactor and cavity geometry and to allow for a homogenous temperature distribution in the membrane-stack reactor (< 50 K difference). The design of the membrane-stack reactor is based on the planar solid-oxide-fuel cell geometry developed by FZJ [3] due to its scalability potential.

2. Simulation of Thermodynamic Limit

2.1 Method

The thermodynamic limit of steam and methane conversion in countercurrent-operated membrane reactors is a crucial factor to identify their potential and to define boundary conditions for operation. The model assumes an ideal membrane, which does not inhibit any transport resistance regarding oxygen ions. The premise for operation is, that there is always an oxygen partial pressure gradient across the membrane. This is fulfilled as long as the oxygen partial pressure on the sweep side $pO_{2,s}$ is < the pressure on the feed side $pO_{2,f}$. The procedure for determining the thermodynamic limit is based on the work and code provided by Bulfin [4], which applies the Gibbs minimization approach using Cantera [5] with the gri30 reaction mechanism.

2.2 Operation Conditions

The use of a reducing agent such as (bio)methane, can drastically lower the oxygen partial pressure on the permeate side of the membrane and consequently also the optimal temperature of the reaction. This effect is so significant that, from a thermodynamic point of view, full conversion of the steam could even be expected below 500 °C with a corresponding methane/steam ratio (see Figure 1). However, this is excluding any kinetic considerations and

oxygen transport effects through the membrane, which influence the obtainable conversion extent [6]. Since (bio)methane is also to be converted into valuable syngas as a by-product, it is worth taking a look at the methane conversion on the permeate side (Figure 2). An optimum range of molar flow ratio and temperature to maximize the methane conversion can be observed. The temperatures should reach at least 750 °C for a conversion above 90%, or 900 °C for up to 98% conversion of methane. Ideally, the molar material flow ratio of methane/H_2O should be as low as possible. Our analysis of the conversion at the thermodynamic limit shows an optimum ratio of around 1. If this value is undercut, both the steam and methane conversion drop significantly.

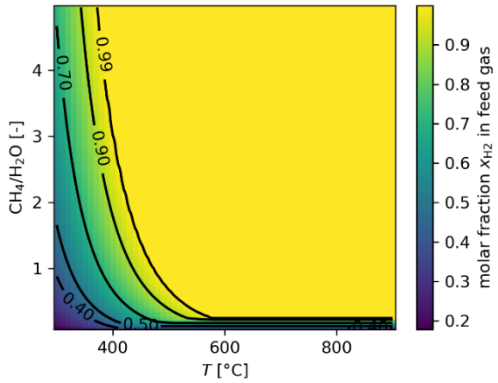

Figure 1. *Conversion of Steam to Hydrogen on the feed gas side as a function of temperature and molar flow ratio (CH_4/H_2O).*

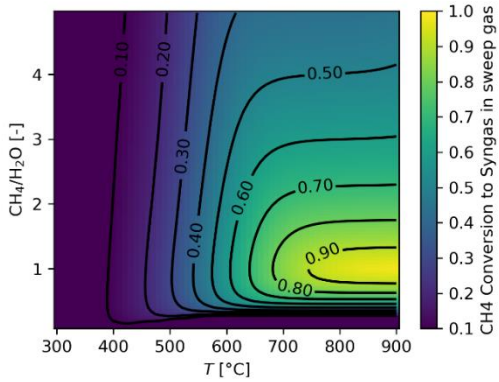

Figure 2. *Methane conversion in the sweep gas as a function of operation temperature and molar flow ratio (CH_4/H_2O).*

An alternative way to reduce the oxygen partial pressure on the permeate side is to use a sweep gas. Here, an inert gas is introduced to dilute the gas composition on the permeate side to such an extent that the partial pressure gradient across the membrane is maintained. The maximum thermodynamically achievable conversion of steam as a function of the molar flow ratio of sweep to feed gas and the temperature is shown in Figure 3 for an approximately pure sweep gas (assuming pO_2 of 10^{-25} Pa). Compared to the case with methane, the temperature must increase significantly to at least 1500 °C to enable water splitting. The molar quantity of sweep gas introduced has a decisive influence on the conversion, e.g. a conversion of 10% can be achieved from a ratio of 5000 at 1500 °C. The oxygen impurity effect for an exemplary ratio of 10^5 is depicted in Figure 4, which highlights the importance of decreasing the oxygen partial pressure in the sweep gas to at least 0.1 Pa.

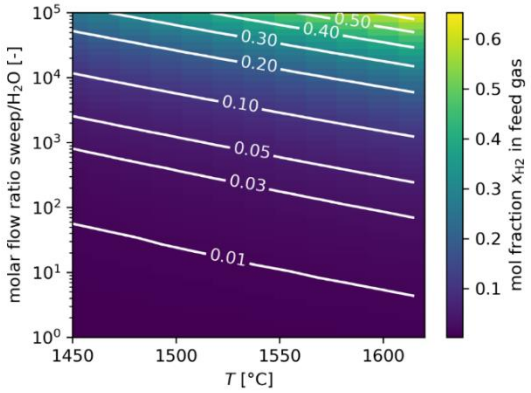

Figure 3. *Steam conversion in a countercurrent membrane reactor with sweep gas (pO_2: 10^{-25} Pa) at thermodynamic limit. Variation of molar flow ratio and temperature.*

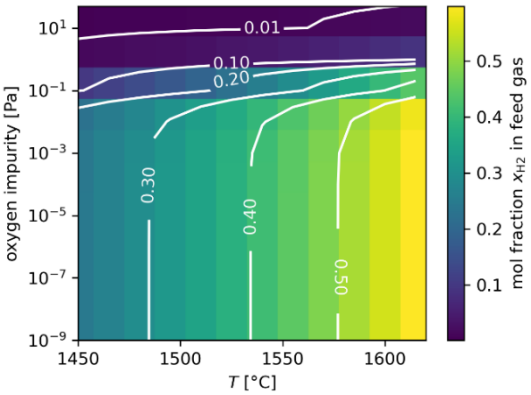

Figure 4. *Steam conversion in a countercurrent membrane reactor with sweep gas at molar flow ratio of 10^5. Variation of oxygen impurity in sweep gas and temperature.*

3. Simulation of Solar Heat Integration

The experimental demonstration of the technology is envisaged at DLR's solar simulator in Cologne with its specific flux distribution [7]. The design of the solar heat integration is based on the approach by Kadohiro et al. [8]. The aim of the solar simulation is to ensure that the set temperature is reached (average reactor temperature between 800 °C and 900 °C) and that the temperature difference in the reactor is < 50 K. The latter is a measure to reduce the risk of membrane-joining failure do to different chemical expansion in the reactor. Figure 5 shows the coupled system of 1D model (to calculate the convection heat losses in the cavity) and the 3D cavity heat transfer model, which integrates ray-tracing and heat transfer methods (conduction, convection, radiation). The convection losses inside the cavity are estimated using the procedure described by Clausing [9]. These convection losses are then assigned as an inlet parameter of the 3D cavity heat transfer model. The average wall temperatures of the two models are compared and the iterative process is performed until the solution converges (deviation < 1%).

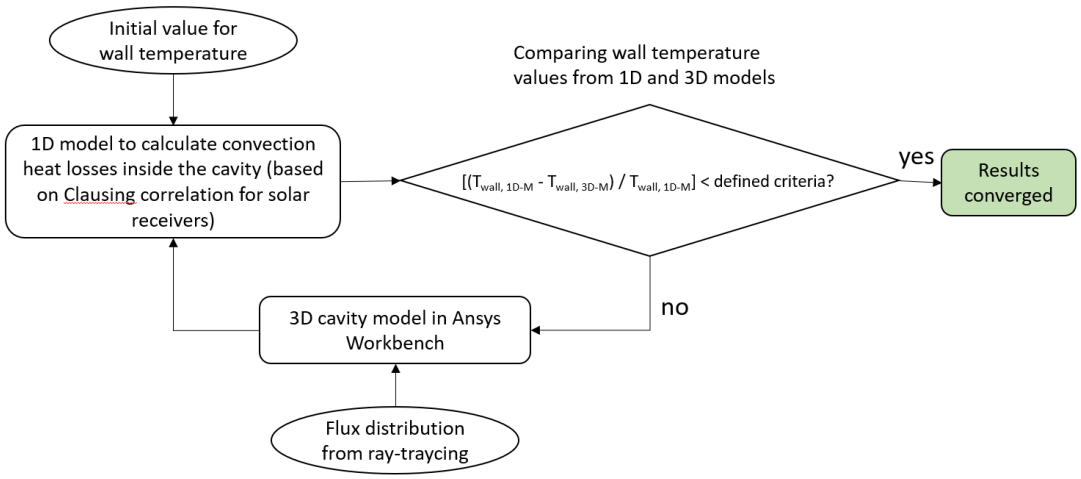

Figure 5. *Coupled system of 1D model (convection heat losses calculation) and 3D cavity model (conduction, convection, radiation).*

3.1 Method

Figure 6 describes the modelled geometry, where the cavity consists of six insulation thermal bricks (Altraform® KVS, wall thickness of 100 mm, emissivity of 0.8), which are configurated to form an inner cubical shape (280 x 280 x 220 mm). The aperture through which the solar radiation enters the cavity is located in the front wall, and its diameters was varied between 40 and 100 mm in this numerical study. The reactor is modelled as a stainless-steel block (25 x 220 x 120 mm, emissivity of 0.5), and three plates (thickness of 10 mm, emissivity of 0.5) are placed at the bottom, front and top of the reactor to homogenise the temperature distribution in this component. Materials with high thermal conductivity in the temperature range of interest 800 – 900 °C are analysed as candidates for the irradiated plates. The emissivity values correspond to the thermal emissivity of oxidised metals and refractory materials in the temperature range between 850 and 1100 °C [10]. The distance from the irradiated plate to the inner side of the front wall corresponds to 165 mm.

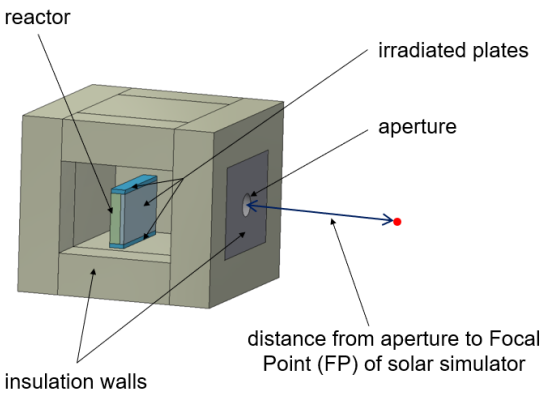

Figure 6. *Model geometry used for the simulations. The side wall is not shown to visualise the components inside the cavity. The focal point of the solar simulator is represented with the red point.*

The cavity was modelled in 3D using the thermal module of the Ansys® Academic Research Workbench 2022 R1 software. To generate the solar heat for the model, the measured flux distribution obtained with one (2.04 kW) and two lamps (3.09 kW) of the solar simulator in Cologne is used. The measured data is modelled with the tools FEMRAY and SPRAY, which are combined with Ansys mechanical APDL for assigning the heat flux to the geometry mesh. For simulating the heat losses to the environment, radiation and convection boundary condi-

tions are assigned to the outer surfaces of the cavity. Natural convection (5 kW/m²) is considered in this calculation. A heat sink condition (-100 W) is assigned to the reactor body to represent the heat demand of the thermochemical process inside the reactor. To represent the heat losses by convection inside the cavity (calculated with the 1D model), a heat flow condition was defined for the surface areas that would come in contact with the air mass flow entering through the cavity aperture.

A mesh analysis with element sizes of 0.005, 0.010, 0.012, 0.020 and 0.030 m was carried out to study the mesh dependency of the model. From this analysis, the mesh with an element size of 0.012 m was selected because the deviation of the average temperature of the reactor (which is defined as the target value of the simulations) was less than 1.5% compared with the finest mesh (0.005 m). The simulation times for the 0.005 and 0.012 m meshes were 1326 and 19761 s, respectively.

3.2 Results

3.2.1 Effect of Plate Material

Thermal simulations were performed with the thermal power of one lamp (2.04 kW) of the solar simulator to analyse the effects of the material plates on the temperature distribution of the reactor. The ray-tracing analysis for an aperture of 60 mm reveals, that 0.53 kW is reflected by the cavity and 1.51 kW enters through the aperture. Figure 7 shows the temperature distribution results from the 3D cavity model with Cu as irradiated plate material.

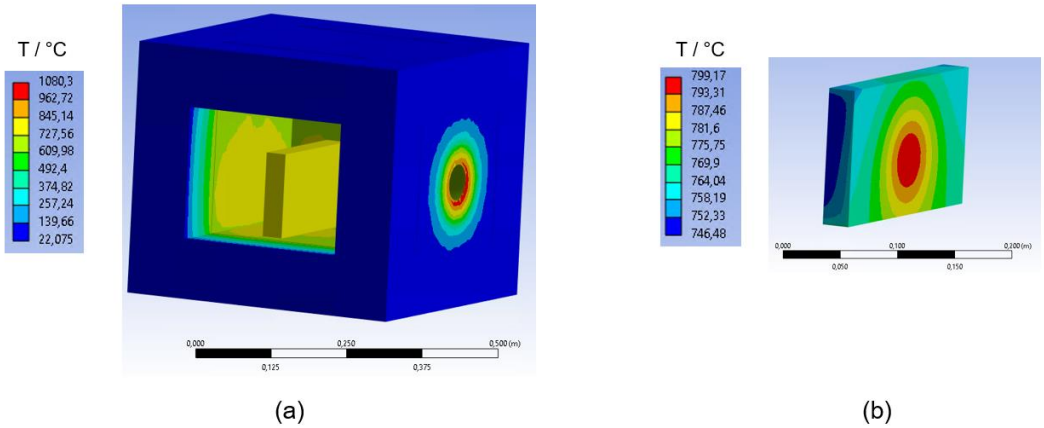

Figure 7. *Temperature distribution in the cavity (a) and reactor (b) for an aperture diameter of 60 mm with the power of one lamp of the solar simulator (2.04 kW) and irradiated plates made of copper.*

The region around the aperture has the highest temperature in the system (1080 °C), which is due to the heating of the thermal insulation by the reflected incident power. A hot spot can be observed in the central area of the reactor which is caused by the peak of the incident radiation. The temperature gradient and the maximum temperature of the reactor are 799.2 °C and 53 K, respectively.

The main function of the irradiated plates is to improve the temperature distribution along the reactor body, which is essential due to the high temperature homogeneity requirements. Therefore, materials with high thermal conductivity in the temperature range of interest (800 – 900 °C) must be selected. We analysed the suitability of copper (thermal conductivity of 350 W/(mK) [11, 12], melting point 1084 °C) silicon carbide (SiC, thermal conductivity of 83 W/(mK)) [11, 12]) regarding the achievable temperatures of the reactor and plate. As expected, the higher the thermal conductivity of the irradiated plates, the more homogeneous is the temperature in the reactor (see orange bar in Figure 8 depicting the maximum temperature difference). While the average temperature of the reactor was the same in all three cases, the

maximum temperature in the irradiated plates was different. This effect is related to the ability of the plate material to conduct and transfer heat. For the planned experimental demonstration, copper was chosen as the material for the irradiated plates and is thus also used for the simulations presented in the next sections.

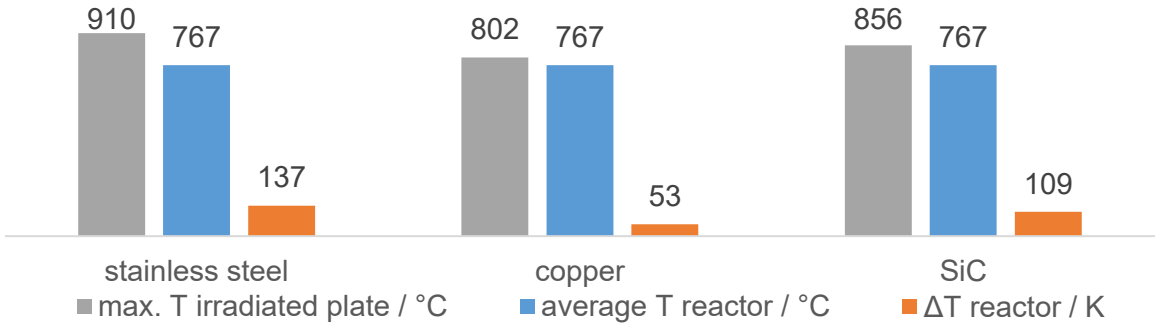

Figure 8. *Simulations results for different irradiated plates materials. Aperture diameter: 60 mm.*

3.2.2 Effect of Cavity Diameter

In order to meet the requirement of a temperature gradient in the reactor of less than 50 K, the diameter of the cavity aperture is optimised. The simulations were carried out using i) one lamp of the solar simulator, ii) irradiated copper plates and iii) aperture diameters of 40, 55, 60, 70 and 100 mm. The obtained results are shown in Table 1. Increasing the aperture diameter led to a higher power inside the cavity. However, this did not result into a higher temperature in the reactor, since the thermal losses also depend on the aperture diameter. The highest average temperature in the reactor (787 °C) was achieved with the aperture diameter of 70 mm. The temperature gradient in the reactor decreases with the aperture diameter. The lowest temperature gradient was 32 K for the geometry with 60 mm aperture diameter, but due to the power reflected by the cavity (27.19% of the thermal power of the lamp), high temperatures in the insulation material (1262 °C) and low average temperatures in the reactor (669 °C) are obtained. A cavity with a diameter of 55 mm allows a temperature gradient below 50 K, but to achieve higher temperatures in the reactor, the incident thermal power must be increased.

Table 1. *Simulation results obtained by changing the aperture diameter of the cavity.*

aperture diameter / mm	(power inside receiver / Total power of lamp)*100	power inside cavity / kW	average T reactor / °C	ΔT reactor / K	max. T reactor	max. T in insulation material
100	82.93	1.69	746	69	785	892
70	78.52	1.60	787	61	823	985
60	74.10	1.51	767	53	799	1072
55	71.16	1.45	752	49	781	1129
40	62.81	1.28	669	32	688	1262

3.2.3 Effect of Distance to Focal Point

In this section, the effect of defocusing the cavity (aperture diameter: 55 mm) from the focal point is used to analyse the effects of changing the incident thermal power in the system while keeping the thermal flux of the lamps constant (2 lamps, thermal power of 3.93 kW).

When the cavity is placed at the focal point of the solar simulator, about 72.72% of the thermal power of the two lamps enters the cavity (Figure 9). However, the 2.86 kW entering the cavity results in a reactor temperature of about 1071 °C, which is very close to the melting point of the copper plates and higher than the required temperature of the reactor. By moving the cavity away from the focal point, the power entering the cavity is reduced, e.g. to 2.85 kW

at a distance of 135 mm resulting in an average temperature of 838 °C. As the distance increases, a reduction in the maximum temperature gradient in the reactor is also observed. This effect is due to lower flux distribution hitting the plate surface when the cavity is defocussed.

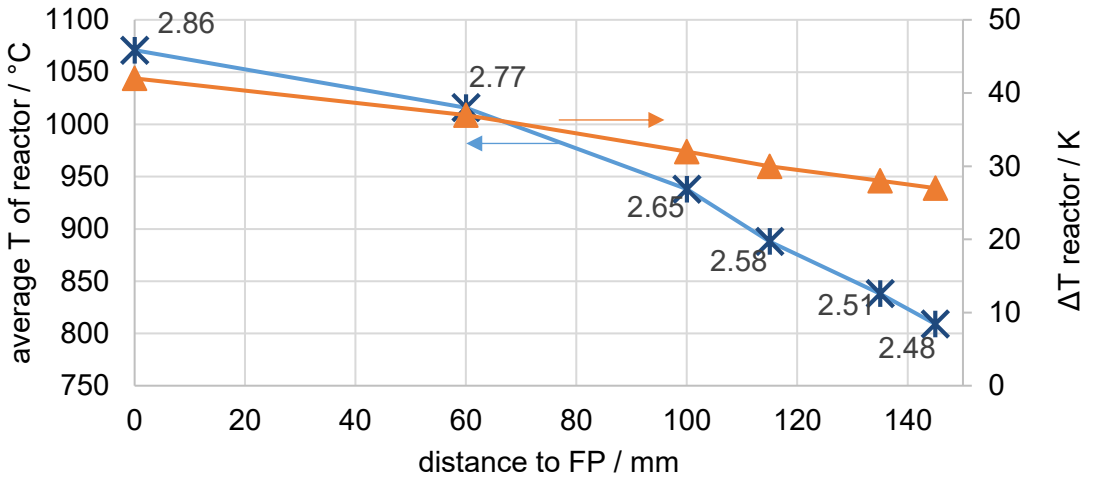

Figure 9. *Results from simulations using two lamps (thermal power of 3.93 kW), a cavity aperture of 55 mm diameter and varying the distance between the aperture and the focal point of the solar simulator. The numbers at the data points refer to the power entering the cavity in kW.*

4. Conclusion and Outlook

The thermodynamic limit analysis showed a high potential for the case of biomethane acting as reducing agent. The operation temperatures need to be at least at 800 °C to ensure a high methane conversion into syngas above 90%. In contrast, for the H_2O splitting with nitrogen as purge gas, the temperatures need to rise at least up to 1500 °C and the requirement of high molar flow rates with low oxygen concentration (< 0.1 Pa) needs to be fulfilled. For the planned experiments at 800 °C to 900 °C with biomethane as reducing agent, a model was developed to design a cavity system that fulfils the temperature requirements for a proof-of-concept membrane reactor. The solar thermal heat is implemented as an inlet boundary condition of the system using measurement data from the solar simulator at the DLR in Cologne. With the help of the model, the geometrical and material parameters of the system were optimised in order to determine both the average temperature and the maximum temperature gradient of the reactor. For the analysed geometry, an aperture of 55 mm and a distance between cavity aperture and the focal point of the solar simulator of 135 mm results in an average temperature of 838 °C with a temperature gradient of about 28 K. Optimising the thermal efficiency of the system was not the focus of this study. However, the reflected power of the system can be used to preheat the educts of the thermochemical process, e.g. by positioning a spiral pipe system around the aperture.

Data availability statement

All of the underlying data and method is publicly available and has been cited where used.

Author contributions

Nicole Carina Neuman: Conceptualization, Methodology, Investigation, Visualization, Writing – original draft, Writing – review & editing. **Juan Pablo Rincon Duarte**: Conceptualization, Methodology, Investigation, Visualization, Writing – original draft, Writing – review & editing. **Martin Roeb**: Funding, Writing – review & editing.

Competing interests

The authors declare that they have no competing interests.

Funding

The authors wish to thank the Federal Ministry of Education and Research in Germany for funding (Funding Code: 03SF0648A).

Acknowledgement

The authors wish to thank Brendan Bulfin for his support in setting up the thermodynamic limit model, Yasuki Kadohiro and Jana Barabas for their guidance regarding solar flux modelling, and Christian Willsch for the measurements of the solar flux distribution.

References

[1] Somtochukwu G. Nnabuife, Eni Oko, Boyu Kuang, Abdulrauf Bello, Azikiwe P. Onwualu, Sherry Oyagha, and James Whidborne. 2023. The prospects of hydrogen in achieving net zero emissions by 2050: A critical review. *Sustainable Chemistry for Climate Action* 2, 100024. DOI: https://doi.org/10.1016/j.scca.2023.100024.

[2] Md M. Rahman, Abayomi O. Oni, Eskinder Gemechu, and Amit Kumar. 2020. Assessment of energy storage technologies: A review. *Energy Conversion and Management* 223, 113295. DOI: https://doi.org/10.1016/j.enconman.2020.113295.

[3] Nigel M. Sammes, Alevtina Smirnova, and Oleksandr Vasylyev. 2005. *Fuel cell technologies*: *State and perspectives*. NATO science series, 202. Springer, Dordrecht.

[4] Brendan Bulfin. 2019. Thermodynamic limits of countercurrent reactor systems, with examples in membrane reactors and the ceria redox cycle. *Physical Chemistry Chemical Physics* 21, 4, 2186–2195. DOI: https://doi.org/10.1039/c8cp07077f.

[5] David G. Goodwin, Harry K. Moffat, Ingmar Schoegl, Raymond L. Speth, and Bryan W. Weber. 2023. *Cantera: An Object-oriented Software Toolkit for Chemical Kinetics, Thermodynamics, and Transport Processes*. Zenodo.

[6] Kai Bittner, Nikolaos Margaritis, Falk Schulze-Küppers, Jörg Wolters, and Ghaleb Natour. 2023. A mathematical model for initial design iterations and feasibility studies of oxygen membrane reactors by minimizing Gibbs free energy. *Journal of Membrane Science* 685, 121955. DOI: https://doi.org/10.1016/j.memsci.2023.121955.

[7] DLR e.V. - Institute of Solar Research, Ed. 2007. *Der neue Hochleistungsstrahler des DLR - Grundlagen, Technik, Anwendung*. DLR e.V. - Institute of Solar Research.

[8] Yasuki Kadohiro, Vamshi K. Thanda, Bruno Lachmann, Kai Risthaus, Nathalie Monnerie, Martin Roeb, and Christian Sattler. 2023. Cavity-shaped direct solar steam generator employing conical helical tube for high-temperature application: Model development, experimental testing and numerical analysis. *Energy Conversion and Management: X* 18, 100366. DOI: https://doi.org/10.1016/j.ecmx.2023.100366.

[9] A. M. Clausing. 1983. Convective Losses From Cavity Solar Receivers - Comparisons Between Analytical Predictions and Experimental Results. *Journal of Solar Energy Engineering1* 105, 29–33.

[10] J. M. Jones, P. E. Mason, and A. Williams. 2019. A compilation of data on the radiant emissivity of some materials at high temperatures. *Journal of the Energy Institute* 92, 3, 523–534. DOI: https://doi.org/10.1016/j.joei.2018.04.006.

[11] Robert P. Minneci, Eric A. Lass, Jeffrey R. Bunn, Hahn Choo, and Claudia J. Rawn. 2021. Copper-based alloys for structural high-heat-flux applications: a review of development, properties, and performance of Cu-rich Cu–Cr–Nb alloys. *International Materials Reviews* 66, 6, 394–425. DOI: https://doi.org/10.1080/09506608.2020.1821485.

[12] Lance L. Snead, Takashi Nozawa, Yutai Katoh, Thak-Sang Byun, Sosuke Kondo, and David A. Petti. 2007. Handbook of SiC properties for fuel performance modeling. *Journal of Nuclear Materials* 371, 1-3, 329–377. DOI: https://doi.org/10.1016/j.jnucmat.2007.05.016.